Am J Transl Res 2022;14(4):2728-2738
www.ajtr.org /ISSN:1943-8141/AJTR0141765

Original Article

Changes in transepithelial electrical resistance and intracellular ion concentration in TGF-β-induced epithelial-mesenchymal transition of retinal pigment epithelial cells

Minli Wang[1], Jiayi Wei[1], Hui Li[1], Fang Wang[1,2]

[1]Department of Ophthalmology, Shanghai Tenth People's Hospital, Tongji University School of Medicine, Shanghai 200072, China; [2]Department of Ophthalmology, Shanghai Bright Eye Hospital, Shanghai 200336, China

Received January 14, 2022; Accepted April 6, 2022; Epub April 15, 2022; Published April 30, 2022

Abstract: Objective: This study aimed to investigate the changes in transepithelial electrical resistance (TEER) and ion concentrations, and their relationship in TGF-β-induced epithelial-mesenchymal transition (EMT) of retinal pigment epithelial (RPE) cells. Methods: RPE cell line ARPE-19 was employed and treated with 10 ng/ml TGF-β1 and TGF-β2 to establish the EMT model *in vitro*. The EMT markers fibronectin, N-cadherin, occludin, zona occludens 1(ZO-1) and claudin-19 were investigated by western blot and immunofluorescence. CellZscope system was used to monitor the TEER values. Fluorescent probe, flow cytometry and automatic microplate reader were employed to detect the changes of Ca^{2+}, Mg^{2+}, Zn^{2+}, Na^+ and K^+ in ARPE-19 cells. Results: The TGF-β1-induced EMT of ARPE-19 cells was marked by the disruption of the distribution of occludin, ZO-1, and claudin-19. The development of TEER was significantly disturbed in both TGF-β1 and TGF-β2 treatment groups. Also, the time course of the maximum slope indicated that the fastest decrease in TEER values occurred after 36 hours. The concentrations of Ca^{2+}, Mg^{2+}, Zn^{2+}, and K^+ increased in TGF-β1- and TGF-β2-treated ARPE-19 cells, while the concentration of Na^+ decreased. Significant inverse correlations were detected between the concentrations of Ca^{2+}, Mg^{2+}, Zn^{2+}, and K^+ and TEER values in ARPE-19 cells treated with TGF-β1. The Na^+ concentration and TEER values showed a positive correlation. Similar results were observed in the TGF-β2 treatment group. The time-effect analysis showed that the concentrations of Ca^{2+}, Mg^{2+}, Zn^{2+} and K^+ increased and peaked after 72, 72, 48, and 72 h, respectively, with the extension of TGF-β1 treatment time. In the TGF-β2 treatment group, the Ca^{2+}, Mg^{2+}, Zn^{2+}, and K^+ concentrations were also upregulated and reached their highest after 72, 72, 72, and 36 h, respectively. In contrast, the concentration of Na^+ decreased and reached the lowest after 48 h in the TGF-β1 treatment group and after 72 h in the TGF-β2 treatment group. Conclusion: TGF-β1 and TGF-β2 disrupted the ARPE-19 cell monolayer, disturbed TJs integrity, downregulated TEER values, and changed intracellular ion permeability. These findings might help further understand the EMT of RPE cells during PVR.

Keywords: Epithelial-mesenchymal transition, ion, retinal pigment epithelial cell, tight junction proteins, transepithelial electrical resistance

Introduction

Proliferative vitreoretinopathy (PVR), which is an exaggerated and protracted scarring process that complicates up to 10% of rhegmatogenous retinal detachment (RRD) cases, is the main reason that leads to failed retinal detachment (RD) surgery [1, 2]. Recent studies indicated that the epithelial-mesenchymal transition (EMT) of retinal pigment epithelium (RPE) cells was the main contributor to the pathogenesis of PVR [3]. In the setting of PVR, RPE cells are activated and undergo EMT, thus achieving the ability to abnormally proliferate, migrate, and produce extracellular matrix components participating in the fibrotic tissue formation [3, 4].

Normally, RPE is a monolayer of highly polarized epithelial cells and is located between the neuroretina and the choroid [5, 6]. The RPE is responsible for maintaining the blood-retina barrier, providing the retina with nutrients, phagocytosing the photoreceptor outer segments, recycling the visual chromophore, and absorbing excess light to prevent photo-oxidation [7]. RPE cells are bound by tight junctions (TJs) [8], adherent junctions (AJs) [9], and gap junctions [10]. TJs, which are the most apically located junctions, play a key role in forming and maintaining the epithelial barrier [1, 11]. They consist of transmembrane proteins claudin and occludin, junctional adhesion molecule-A (JAM-A), and intracellular plaque proteins zonula occludens (ZO) and cingulin [12]. They regulate the transport of macromolecules and ions, including Ca^{2+} [13, 14], Mg^{2+} [14], and Na^{+} [14-16]. Mukaiyama et al. [13] found that Ca^{2+} was transported by TJs in epithelial MDCK II monolayers. Milatz et al. [14] reported that TJs with claudin-19 had a greater effect on the transport of Mg^{2+} than Ca^{2+} in the thick ascending limb of Henle's loop of the kidney.

TEER is widely used to evaluate the integrity of TJ dynamics of epithelial monolayers [17]. The TEER values have high specificity for the permeability of a reactive tightly connected complex. In ophthalmology, the down-regulation of TEER is closely related to RPE barrier dysfunction in diabetic retinopathy [18], glaucoma [19], and corneal diseases [20]. Scuderi et al. [18] showed that the downregulation of TEER due to the disruption of TJs was one of the main factors accounting for diabetic macular edema. Zhang et al. [21] reported that the platelet-activating factor could significantly decrease the TEER of ARPE-19 cells and destroy the barrier functions. Moreover, oxidative stress potentially contributed to RPE dysfunction in aging and related diseases by downregulating TEER in RPE cells [22].

However, the TEER changes in RPE cells during PVR pathology are rarely reported. This study aimed to investigate the changes in TEER and ion concentrations, and their relationship in the EMT of RPE cells induced by TGF-β.

Materials and methods

Cell lines and reagents

The human RPE cell line ARPE-19 in our lab [9, 23, 24] was used in this study. The antibody for detecting occludin was supplied by Invitrogen (CA, USA). Anti-ZO-1 was purchased from Abcam (ON, Canada). Anti-claudin-19 was obtained from Santa Cruz Biotechnology (CA, USA).

Cell culture and treatment

Human RPE cell line ARPE-19 cells were initially grown in a 1:1 mixture of Dulbecco's modified Eagle's medium (DMEM, Gibco, NY, USA) and Ham's F12 medium supplemented with 10% fetal bovine serum (FBS; Gibco) at 37°C in the presence of 5% CO_2. When the cells were at 80%-90% confluency, the concentration of FBS was decreased to 1% to promote the formation of TJs. After 2 weeks, the cells were treated with 10 ng/mL human recombinant TGF-β1 or TGF-β2 (Invitrogen, CA, USA).

Immunofluorescent staining

The immunofluorescent staining was described in detail in our previous study [9, 24]. The stained ARPE-19 cells were observed using an OLYMPUS microscope.

TEER measurement

Polycarbonate membrane Transwell inserts (24-well tissue cultures, 0.4 μm pore size; Costar Corning, CA, USA) were used to mimic the PVR environment *in vitro*. ARPE-19 cells were cultured in DMEM/F12 with 10% FBS in the upper monolayer until they were confluent, and then the FBS concentration was changed to 1% until a TEER > 20 $\Omega \cdot cm^2$ (about 14-18 days) was achieved. Further, TGF-β1 or TGF-β2 was added. An automated cell monitoring CellZscope system (NanoAnalytics, Münster, Germany) was used to monitor TEER, cell layer capacitance (C_{CL}), and medium resistance (Rmed) in real-time. High TEER values reflected tight barriers. C_{CL} was used to evaluate monolayer cells. The lower the C_{CL}, the more the cells grew in the monolayer. Rmed was used to record the resistance of the culture medium.

Flow cytometry analysis

Flow cytometry was used to quantitate the strength of the fluorescent probe of Ca^{2+} (F14021, Thermo Fisher), Mg^{2+} (M3735, Thermo Fisher), Zn^{2+} (F24195, Thermo Fisher), and Na^{+} (C36676, Thermo Fisher), which represented the concentrations of intracellular ions. Briefly, 10,000 cells were examined per sample using a Becton Dickinson FACSCalibur to excite

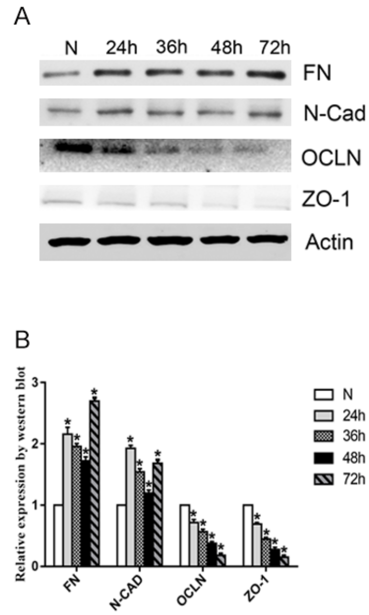

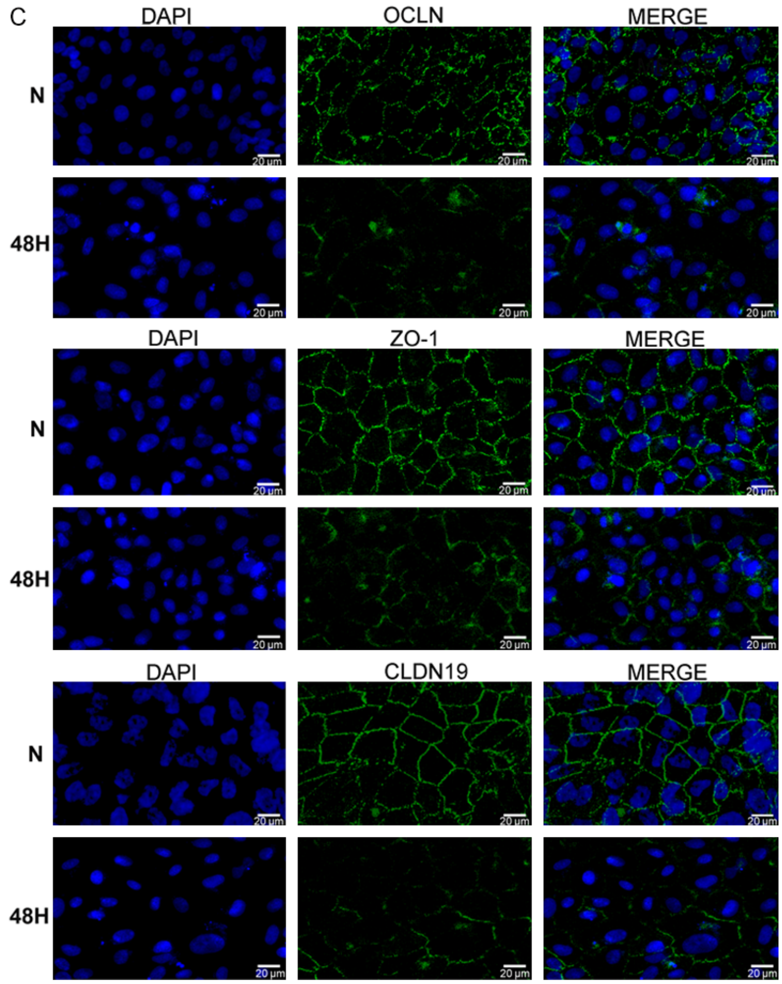

Figure 1. TGF-β1 destroyed the distribution of TJ proteins in ARPE-19 cells. The distribution of TJ proteins occludin, ZO-1, and claudin-19 were detected by immunofluorescence. Representative images of occludin (green), ZO-1 (green), and claudin-19 (green) expression in TGF-β1-treated ARPE-19 cells after 36 h and normal control. DAPI (blue) was used as a nuclear marker. Magnification, 40 ×. Scale bar, 20 μm.

the cells with a 488-nM argon laser, and the collected data obtained were analyzed using Cell QuestTM software (Becton Dickinson, CA, USA).

Automatic microplate reader test

ARPE-19 cells were loaded with the K^+ indicator dye (P1267MP, Thermo Fisher) for 1 h in 96-wells plates (Costar Corning). The ratio of the fluorescence intensities obtained by exciting wavelengths at 340/380 nm and emission at 500 nm was used to determine the concentration of K^+.

Statistical analysis

Prism software (v.6.05; GraphPad Software, CA, USA) was used for performing one-way analysis of variance (ANOVA), Tukey's multiple comparison *post hoc* tests, Pearson product-moment correlation and two-way repeated-measures ANOVA. A P value < 0.05 indicated a significant difference. All values were reported as means ± SEM.

Results

TGF-β1 induced EMT in ARPE-19 cells

TGF-β1 treatment (10 ng/ml) induced the upregulation of the expression of mesenchymal markers fibronectin and N-cadherin and the downregulation of the expression of TJs proteins occludin and ZO-1 in ARPE-19 cells at the protein (**Figure 1A**) and mRNA levels (**Figure 1B**). Additionally, the integrity of TJs was disrupted with the distribution of occludin, ZO-1, and claudin-19 (**Figure 1C**).

TGF-β1 or TGF-β2 decreased TEER in ARPE-19 cells

Figure 2A shows the schematic structure of CellZscope. The Transwell with ARPE-19 cells

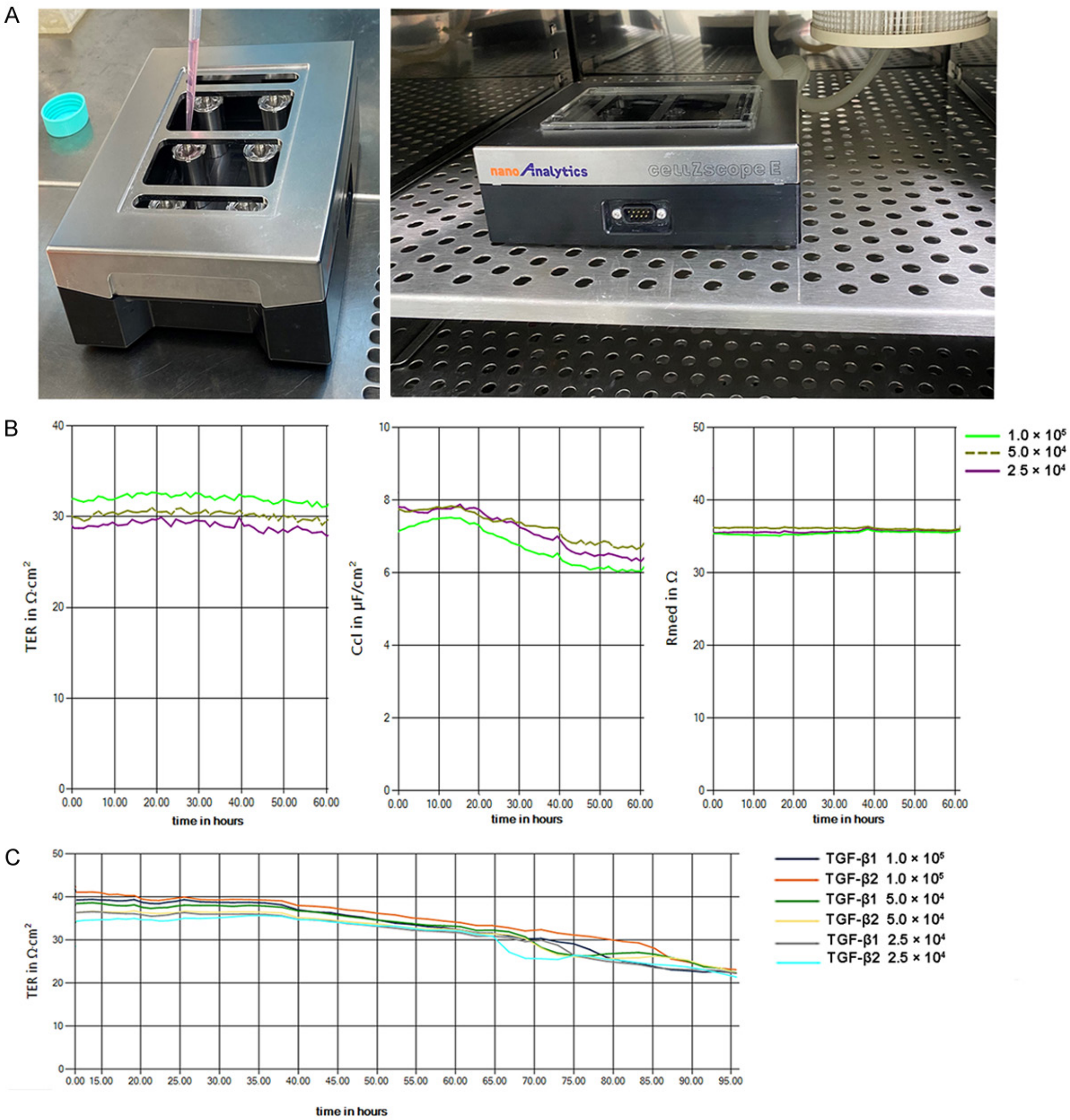

Figure 2. Measurement of TEER. A. Schematic structure and measurement method of the CellZscope. B. When three groups (2.5×10^4 cells/ mL, 5.0×10^4 cells/ mL, and 1.0×10^5 cells/mL) of ARPE-19 cells were cultured for 2 weeks, the CellZscope was used to record TEER, C_{CL} and Rmed values. C. TEER values in the three groups (2.5×10^4 cells/mL, 5.0×10^4 cells/mL and 1.0×10^5 cells/mL) decreased using TGF-β1 and TGF-β2.

was seated in a stainless-steel pot that acted as an electrical conductor, and the second electrode suspended over the cells made contact with the media in the apical chamber. The whole set was put in a sterile, humidified, 37°C, and 5% CO_2 incubator, and the TEER was monitored in real time. For exploring the highest resistance values, three groups of ARPE-19 cells with different densities (1×10^5 cells/mL, 5×10^4 cells/mL, and 2.5×10^4 cells/mL) were investigated. The changes in TEER, cell layer capacitance (C_{CL}), and medium resistance (Rmed) in the three groups at different time points are shown in **Figure 2B**. The highest TEER values were observed in the 1×10^5 cells/mL group (32.62 ± 0.5 Ω.cm²), followed by 5×10^4 cells/mL (30.61 ± 0.3 Ω.cm²) and 2.5×10^4 cells/mL (29.90 ± 0.6 Ω.cm²) groups. The trend of C_{CL} in the three groups was opposite to that of TEER. The Rmed values in the three groups remained steady, with no obvious differences in each group (**Figure 2B**). TGF-β1 and TGF-β2 treatment resulted in a decrease in TEER in ARPE-19 cells in all groups. The time course of maximum slope indicated that the TEER values decreased the fastest in 36 h in the three groups (**Figure 2C**).

Changes in intracellular ion concentrations

The concentrations of Ca^{2+} (**Figure 3A** and **3B**), Mg^{2+} (**Figure 3C** and **3D**), Zn^{2+} (**Figure 3E** and **3F**), Na^{+} (**Figure 3G** and **3H**) and K^{+} (**Figure 3I** and **3J**) in ARPE-19 cells were detected after TGF-β1 and TGF-β2 treatment at different time points. In TGF-β1-treated group, the concentrations of intracellular Ca^{2+}, Mg^{2+}, Zn^{2+}, and K^{+} increased, while the concentration of Na^{+} decreased. Among these, the concentrations of Ca^{2+} and Mg^{2+} in ARPE-19 cells reached peaks after 72 h. The effect of TGF-β2 treatment was the same as that of TGF-β1 (**Figure 3F** and **3J**).

Correlation analysis between the concentrations of intracellular Ca^{2+}, Mg^{2+}, Zn^{2+}, K^{+}, and Na^{+} and TEER

Under the treatment of TGF-β1, the concentration of Ca^{2+} (r = -0.90, P = 0.03), Mg^{2+} (r = -0.90, P = 0.01), Zn^{2+} (r = -0.96, P = 0.01), and K^{+} (r = -0.89, P = 0.04) strongly negatively correlated with TEER values, and that of Na^{+} (r = 0.99, P = 0.01) highly positively correlated with TEER values (**Figure 4A-E**). Under TGF-β2 treatment, the ion concentrations of Ca^{2+} (r = -0.84, P = 0.04), Mg^{2+} (r = -0.81, P = 0.04), Zn^{2+} (r = -0.83, P = 0.04), and K^{+} (r = -0.91, P = 0.03); TEER values also showed a significant negative correlation. The Na^{+} concentration strongly positively correlated with TEER values (r = 0.96, P = 0.01) (**Figure 4F-J**).

Time-effect analysis of intracellular Ca^{2+}, Mg^{2+}, Zn^{2+}, K^{+}, and Na^{+} at different time points after TGF-β treatment

With the extension of TGF-β1 treatment time, the concentrations of Ca^{2+}, Mg^{2+}, Zn^{2+}, and K^{+} increased and peaked after 72 h (186%), 72 h (210%), 48 h (136%), and 72 h (125%) respectively (**Figure 5A-D**). However, in the TGF-β2 group, the concentrations of Ca^{2+}, Mg^{2+}, Zn^{2+}, and K^{+} were also upregulated and reached the highest after 72 h (312%), 72 h (206%), 72 h (225%), and 36 h (138%), respectively (**Figure 5F-I**). Interestingly, the Na^{+} concentration decreased and reached the lowest after 48 h in the TGF-β1 (15%) treatment group and after 72 h in the TGF-β2 (13%) treatment group (**Figure 5E** and **5J**).

Discussion

RPE cells undergo EMT following retinal detachment, playing a key role in the formation of fibrous tissue on the surface of the retina and the vitreous cavity [25]. Our previous studies [2, 3, 9, 26, 27] successfully built an RPE cell EMT model *in vitro* using TGF-β treatment and identified that TGF-β played a critical role in the development of EMT in RPE cells [2]. We also demonstrated that the expression of many junction-related proteins between RPE cells changed before the occurrence of EMT in RPE cells [24]. The most significant change was the reversal of the expression of E-cadherin and N-cadherin proteins. That is, the expression of E-cadherin protein was downregulated while the expression of N-cadherin protein was upregulated, indicating the prelude and biomarker to EMT in RPE cells. The present study aimed to investigate changes in the ion concentration after the integrity of the RPE monolayer was damaged, accompanied by the abnormal expression of junction-related proteins in RPE cells. We used the CellZscope method and fluorescent probe to examine the changes in TEER and ion concentration in TGF-β-induced EMT of RPE cells. Our study found that the 1 × 10^5 ARPE-19 cells/mL group had the highest TEER values and the lowest C_{CL}. The TEER values of ARPE-19 cells gradually decreased in both TGF-β1 and TGF-β2 treatment groups. Also, the time course of the maximum slope indicated that the TEER values dropped at the fastest rate in 36 h. The barrier function of epithelial cells was rarely reported. Balda et al. reported that the overexpression of occludin could increase TEER values [28]. Claudin can directly affect the TEER and determine the ion selectivity of TJs [29]. TJ proteins may influence epithelial resistance. In 2014, Czupalla et al. [30] used the CellZscope to monitor the primary mouse brain microvascular endothelial cells in a recent investigation on the blood-brain barrier (BBB). They indicated that the primary mouse brain microvascular endothelial cells showed a gradual increase in TEER values and a decrease in C_{CL} until reaching a plateau, indicating the monolayer confluency. This study was the first

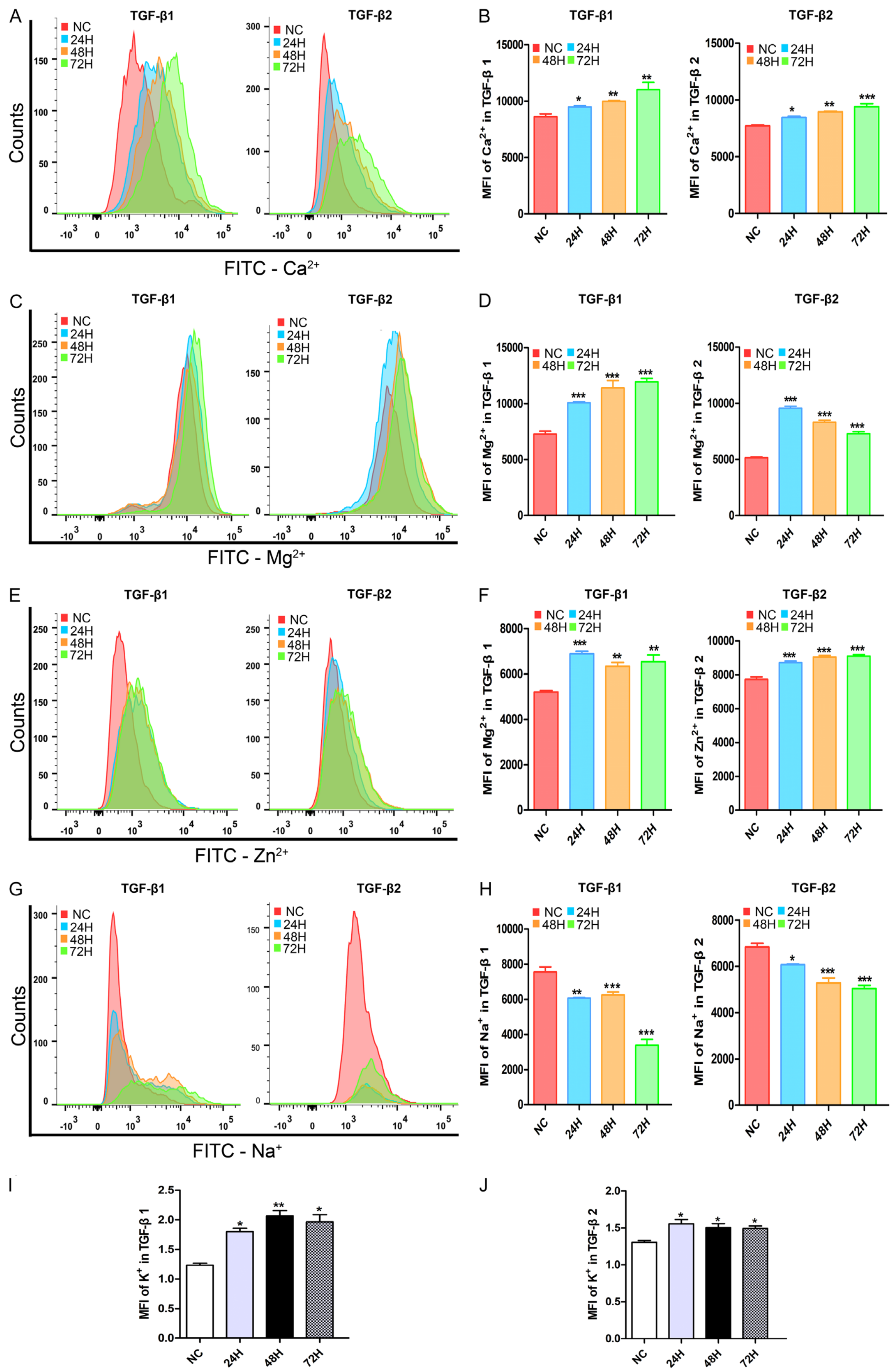
A
TGF-β1
TGF-β2
NC
24H
48H
72H
Counts
FITC - Ca2+
B
TGF-β1
TGF-β2
MFI of Ca2+ in TGF-β 1
MFI of Ca2+ in TGF-β 2
NC
24H
48H
72H
C
TGF-β1
TGF-β2
Counts
FITC - Mg2+
D
TGF-β1
TGF-β2
MFI of Mg2+ in TGF-β 1
MFI of Mg2+ in TGF-β 2
E
TGF-β1
TGF-β2
Counts
FITC - Zn2+
F
TGF-β1
TGF-β2
MFI of Mg2+ in TGF-β 1
MFI of Zn2+ in TGF-β 2
G
TGF-β1
TGF-β2
Counts
FITC - Na+
H
TGF-β1
TGF-β2
MFI of Na+ in TGF-β 1
MFI of Na+ in TGF-β 2
I
MFI of K+ in TGF-β 1
J
MFI of K+ in TGF-β 2

Figure 3. Intracellular concentrations of Ca^{2+}, Mg^{2+}, Zn^{2+}, Na^{+}, and K^{+} were determined using fluorescent probes by flow cytometry and automatic microplate reader. A-J. Measurement of intracellular concentrations of Ca^{2+}, Mg^{2+}, Zn^{2+}, and Na^{+} using the fluorescent probe by flow cytometry. *Left*, representative flow cytometric histogram of fluorescent levels. *Right*, quantification of intracellular ions levels from three independent experiments. I and J. Quantification of the K^{+} concentrations in TGF-β1-treated and TGF-β2-treated groups using an automatic microplate reader after fluorescent probe staining. $^{*}P < 0.05$; $^{**}P < 0.01$; $^{***}P < 0.001$.

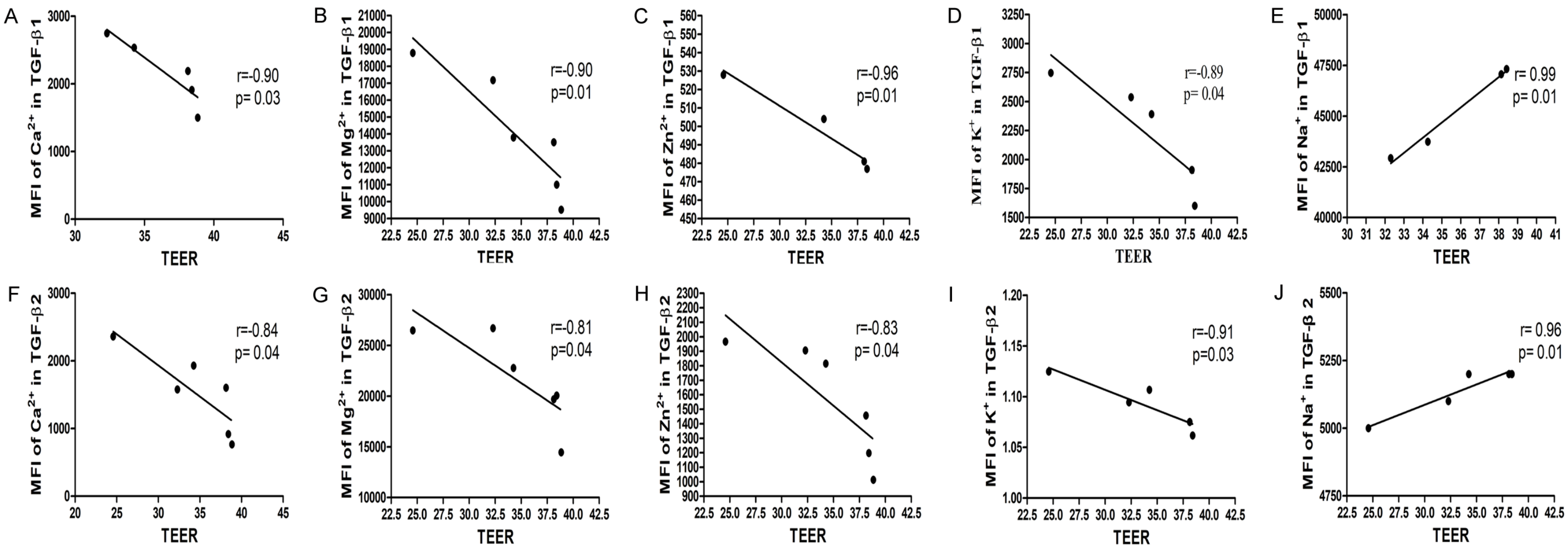

Figure 4. Correlation analysis between intracellular concentrations of Ca^{2+}, Mg^{2+}, Zn^{2+}, K^{+}, Na^{+} and TEER values. A-E. Correlation analysis between intracellular concentrations of Ca^{2+}, Mg^{2+}, Zn^{2+}, K^{+}, Na^{+} and TEER changes in the TGF-β1 group. F-J. Correlation analysis between intracellular concentrations of Ca^{2+}, Mg^{2+}, Zn^{2+}, K^{+}, Na^{+} and TEER values in the TGF-β2 group.

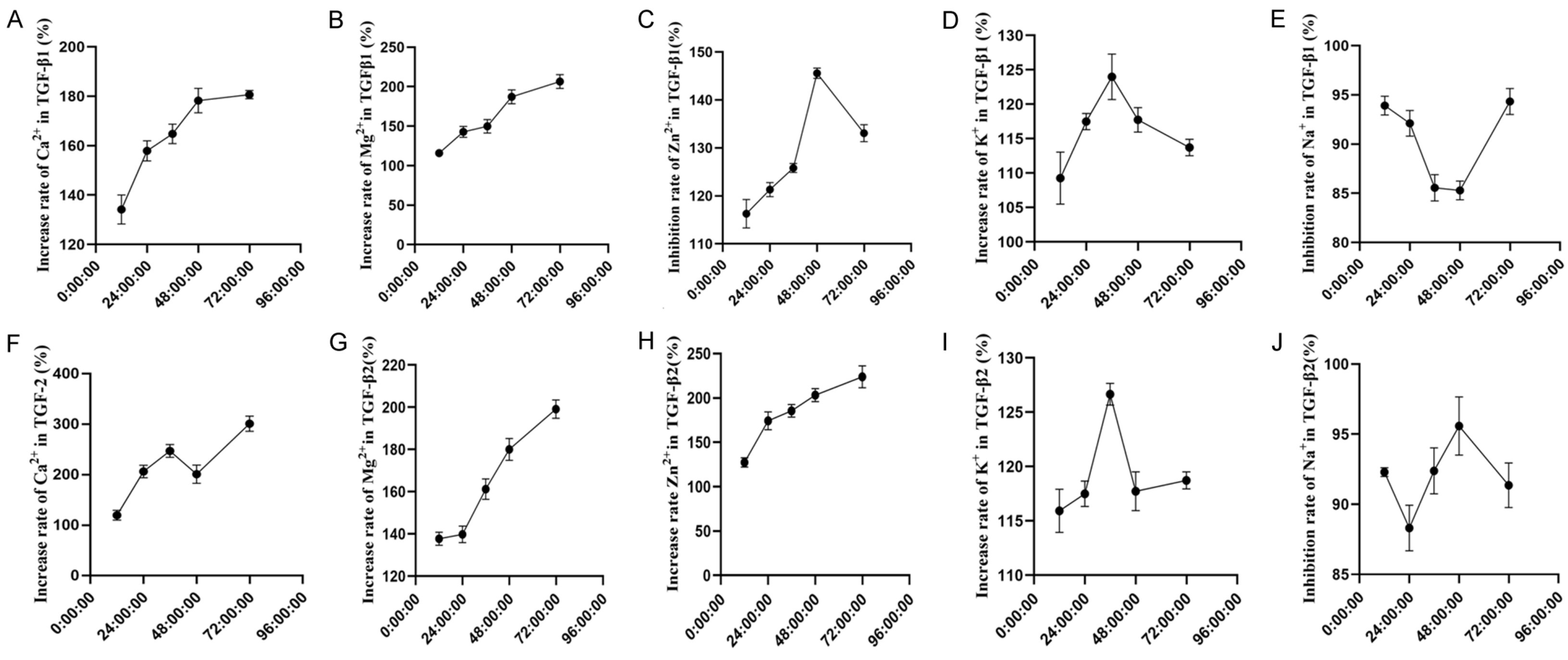

Figure 5. Time-effect analysis of intracellular concentrations of Ca^{2+}, Mg^{2+}, Zn^{2+}, K^{+}, and Na^{+} after treatment with TGF-β1 and TGF-β2. A-E. Time-effect analysis of intracellular concentrations of Ca^{2+}, Mg^{2+}, Zn^{2+}, K^{+}, and Na^{+} in the TGF-β1 group. F-J. Time-effect analysis between intracellular concentrations of Ca^{2+}, Mg^{2+}, Zn^{2+}, K^{+}, and Na^{+} in the TGF-β2 group.

report in ophthalmology. Our results basically agreed with those of Czupalla et al. in the BBB.

EMT is characterized by the decreased expression of epithelial markers, such as E-cadherin, ZO-1, occludin, and claudin, and the increased expression of mesenchymal makers, including fibronectin and N-cadherin [26, 31, 32]. ZO-1 connects occludin and claudin proteins to the cytoskeleton and plays an important role in assembling mature TJ structures and maintaining the integrity of the TJ complex [33]. Occludin and claudins determine the permeability and semi-selectivity of TJs [14, 34].

TEER is a good indicator of barrier integrity and is usually used as an effective tool to assess the ion transport and permeability of TJs [31]. Many studies use TEER values to quantitatively evaluate the barrier integrity of cells in different stages of growth and differentiation. At present, three methods are used to measure TEER: EVOM, CellZscope, and organ-on-chips [32]. Compared with EVOM and organ-on-chips, the CellZscope is more reliable and popular. It can provide more information about C_{CL} and Rmed by applying a small-amplitude alternating excitation signal with a frequency scan [32]. The accuracy of TEER measurement is influenced by many factors, including the intrinsic characteristics of epithelial cells and external factors, such as the temperature, the number of cell passages, and the composition of the culture medium [33]. Matter et al. [33] found that if MDCK cells were allowed to cool to ambient temperature before TEER measurement, the TEER values would increase by more than one third. Therefore, incubation at 37°C is recommended. In this study, we placed the CellZscope in an incubator, using fixed-passage ARPE-19 cells (9th to 12th passage); no serum was added to the medium to keep Rmed stable and to obtain reliable TEER values.

Metal ions play a key role in a broad range of cellular processes [34-36]. For example, Ca^{2+}, Mg^{2+}, K^+, and Na^+ are essential for maintaining the stability, proper folding, and functioning of RNA and proteins [34, 37, 38]. Our study found that TGF-β1 and TGF-β2 treatment destroyed the TJ structure of ARPE-19 cells and was accompanied by a decrease in TEER values. Next, we detected whether the intracellular ion concentration was affected by TGF-β treatment and its relationship with TEER values. The results showed that the concentrations of Ca^{2+}, Mg^{2+}, Zn^{2+}, and K^+ increased in TGF-β1- and TGF-β2-treated ARPE-19 cells, while the concentration of Na^+ decreased. Among these, the concentrations of Mg^{2+} and Ca^{2+} changed the most in the TGF-β1 and TGF-β2 groups, respectively. Ca^{2+} is well known for the formation of TJs and AJs molecules, such as E-cadherin, at cell-cell junctions [39]. Huang et al. [39] reported that the Ca^{2+} concentration was closely related to the downregulation of ZO-1 and TEER values. Currently, research on the concentrations of Mg^{2+} and Zn^{2+} in the RPE barrier is limited. Lodemann et al. [40] indicated that an increase in the intracellular Zn^{2+} concentration might lead to a decrease in TEER values in Caco-2 cells. The upregulation of the K^+ concentration and downregulation of the Na^+ concentration in TGF-β-induced ARPE-19 cells might be because of the co-transport of Na^+-K^+-ATPase and Na^+-K^+-CL on the surface of RPE [41, 42]. The hyperpolarization of the K^+ channel exceeded the depolarization produced by the K^+-induced inhibition of the Na^+-K^+ pump, and therefore the TEER increased substantially. Additionally, the method of measuring K^+ concentration in our study was different from that of measuring the concentrations of Ca^{2+}, Mg^{2+}, Zn^{2+}, and Na^+. Due to the particularity of the K^+ fluorescent probes, we used a microplate reader instead of flow cytometry to quantify the K^+ concentration.

The increase in ion permeability is accompanied by a drop in the TEER. Some studies confirmed that the Ca^{2+} influx activated the phosphorylation of PLC-γ1, leading to the opening of TJs and the decrease in the TEER [43]. Other studies also found that reducing the TEER could increase the permeation of Na^+ more than twofold on MDCK monolayers [27]. The correlation analysis of this study demonstrated a significant negative correlation between the concentrations of Ca^{2+}, Mg^{2+}, Zn^{2+}, and K^+ and TEER in ARPE-19 cells treated with TGF-β1 and TGF-β2; the Na^+ concentration positively correlated with TEER. The results indicated that the down-regulation of TEER induced by TGF-β1 and TGF-β2 resulted in changes in ion permeability in ARPE-19 cells. Future research will further investigate the underlying molecular mechanism.

In summary, in TGF-β-induced ARPE-19 cell EMT, the destruction of the cell monolayer was accompanied by the downregulation of the TEER values and the changes in the intracellular concentrations of Ca^{2+}, Mg^{2+}, Zn^{2+}, K^{+}, and Na^{+}. Also, the changes in the concentrations of Ca^{2+}, Mg^{2+}, Zn^{2+}, K^{+}, and Na^{+} were significantly related to TEER values. These findings might help further understand the EMT of RPE cells during PVR.

Acknowledgements

This work was supported by the National Natural Science Foundation of China (Nos. 81770939 and 82171077).

Disclosure of conflict of interest

None.

Address correspondence to: Fang Wang and Hui Li, Department of Ophthalmology, Shanghai Tenth People's Hospital, Tongji University School of Medicine, 301 Middle Yanchang Road, Shanghai 200072, China. E-mail: fwangoph@163.com (FW); lihuioph@163.com (HL)

References

[1] Naylor A, Hopkins A, Hudson N and Campbell M. Tight junctions of the outer blood retina barrier. Int J Mol Sci 2019; 21: 211.

[2] Li H, Li M, Xu D, Zhao C, Liu G and Wang F. Overexpression of Snail in retinal pigment epithelial triggered epithelial-mesenchymal transition. Biochem Biophys Res Commun 2014; 446: 347-351.

[3] Yang S, Li H, Li M and Wang F. Mechanisms of epithelial-mesenchymal transition in proliferative vitreoretinopathy. Discov Med 2015; 20: 207-217.

[4] Bastiaans J, van Meurs JC, van Holten-Neelen C, Nagtzaam NM, van Hagen PM, Chambers RC, Hooijkaas H and Dik WA. Thrombin induces epithelial-mesenchymal transition and collagen production by retinal pigment epithelial cells via autocrine PDGF-receptor signaling. Invest Ophthalmol Vis Sci 2013; 54: 8306-8314.

[5] Keeling E, Chatelet DS, Tan NYT, Khan F, Richards R, Thisainathan T, Goggin P, Page A, Tumbarello DA, Lotery AJ and Ratnayaka JA. 3D-reconstructed retinal pigment epithelial cells provide insights into the anatomy of the outer retina. Int J Mol Sci 2020; 21: 8408.

[6] Zhang Y, Wang K, Pan J, Yang S, Yao H, Li M, Li H, Lei H, Jin H and Wang F. Exosomes mediate an epithelial-mesenchymal transition cascade in retinal pigment epithelial cells: implications for proliferative vitreoretinopathy. J Cell Mol Med 2020; 24: 13324-13335.

[7] Brown EE, DeWeerd AJ, Ildefonso CJ, Lewin AS and Ash JD. Mitochondrial oxidative stress in the retinal pigment epithelium (RPE) led to metabolic dysfunction in both the RPE and retinal photoreceptors. Redox Biol 2019; 24: 101201.

[8] Tamiya S, Liu L and Kaplan HJ. Epithelial-mesenchymal transition and proliferation of retinal pigment epithelial cells initiated upon loss of cell-cell contact. Invest Ophthalmol Vis Sci 2010; 51: 2755-2763.

[9] Yang S, Yao H, Li M, Li H and Wang F. Long noncoding RNA MALAT1 mediates transforming growth factor Beta1-induced epithelial-mesenchymal transition of retinal pigment epithelial cells. PLoS One 2016; 11: e0152687.

[10] Akanuma SI, Higashi H, Maruyama S, Murakami K, Tachikawa M, Kubo Y and Hosoya KI. Expression and function of connexin 43 protein in mouse and human retinal pigment epithelial cells as hemichannels and gap junction proteins. Exp Eye Res 2018; 168: 128-137.

[11] Jin SW, Lee GH, Pham HT, Choi JH and Jeong HG. Polyhexamethylene guanidine phosphate damages tight junctions and the F-actin architecture by activating calpain-1 via the P2RX7/Ca(2+) signaling pathway. Cells 2019; 9: 59.

[12] Citi S, Sabanay H, Jakes R, Geiger B and Kendrick-Jones J. Cingulin, a new peripheral component of tight junctions. Nature 1988; 333: 272-276.

[13] Mukaiyama M, Usui T and Nagumo Y. Non-electrophilic TRPA1 agonists, menthol, carvacrol and clotrimazole, open epithelial tight junctions via TRPA1 activation. J Biochem 2020; 168: 407-415.

[14] Milatz S, Himmerkus N, Wulfmeyer VC, Drewell H, Mutig K, Hou J, Breiderhoff T, Muller D, Fromm M, Bleich M and Gunzel D. Mosaic expression of claudins in thick ascending limbs of Henle results in spatial separation of paracellular Na+ and Mg2+ transport. Proc Natl Acad Sci U S A 2017; 114: E219-E227.

[15] Chen CC, Marshall WS, Robertson GN, Cozzi RRF and Kelly SP. Mummichog gill and operculum exhibit functionally consistent claudin-10 paralog profiles and Claudin-10c hypersaline response. Biol Open 2021; 10: bio058868.

[16] Inge LJ, Rajasekaran SA, Yoshimoto K, Mischel PS, McBride W, Landaw E and Rajasekaran AK. Evidence for a potential tumor suppressor role for the Na,K-ATPase beta1-subunit. Histol Histopathol 2008; 23: 459-467.

[17] Srinivasan B, Kolli AR, Esch MB, Abaci HE, Shuler ML and Hickman JJ. TEER measurement techniques for in vitro barrier model systems. J Lab Autom 2015; 20: 107-126.

[18] Scuderi S, D'Amico AG, Castorina A, Imbesi R, Carnazza ML and D'Agata V. Ameliorative effect of PACAP and VIP against increased permeability in a model of outer blood retinal barrier dysfunction. Peptides 2013; 39: 119-124.

[19] Watanabe M, Ida Y, Ohguro H, Ota C and Hikage F. Establishment of appropriate glaucoma models using dexamethasone or TGFbeta2 treated three-dimension (3D) cultured human trabecular meshwork (HTM) cells. Sci Rep 2021; 11: 19369.
[20] Kabashima K, Murakami A and Ebihara N. Effects of benzalkonium chloride and preservative-free composition on the corneal epithelium cells. J Ocul Pharmacol Ther 2020; 36: 672-678.
[21] Zhang F, Liu L, Zhang H and Liu ZL. Effect of platelet-activating factor on barrier function of ARPE-19 cells. Drug Des Devel Ther 2020; 14: 4205-4214.
[22] Nicholson C, Shah N, Ishii M, Annamalai B, Brandon C, Rodgers J, Nowling T and Rohrer B. Mechanisms of extracellular vesicle uptake in stressed retinal pigment epithelial cell monolayers. Biochim Biophys Acta Mol Basis Dis 2020; 1866: 165608.
[23] Yao H, Li H, Yang S, Li M, Zhao C, Zhang J, Xu G and Wang F. Inhibitory effect of bone morphogenetic protein 4 in retinal pigment epithelial-mesenchymal transition. Sci Rep 2016; 6: 32182.
[24] Bao H, Yang S, Li H, Yao H, Zhang Y, Zhang J, Xu G, Jin H and Wang F. The interplay between E-cadherin, connexin 43, and zona occludens 1 in retinal pigment epithelial cells. Invest Ophthalmol Vis Sci 2019; 60: 5104-5111.
[25] Boles NC, Fernandes M, Swigut T, Srinivasan R, Schiff L, Rada-Iglesias A, Wang Q, Saini JS, Kiehl T, Stern JH, Wysocka J, Blenkinsop TA and Temple S. Epigenomic and transcriptomic changes during human RPE EMT in a stem cell model of epiretinal membrane pathogenesis and prevention by nicotinamide. Stem Cell Reports 2020; 14: 631-647.
[26] Li H, Wang H, Wang F, Gu Q and Xu X. Snail involves in the transforming growth factor beta1-mediated epithelial-mesenchymal transition of retinal pigment epithelial cells. PLoS One 2011; 6: e23322.
[27] Zhang Y, Zhou S, Deng F, Chen X, Wang X, Wang Y, Zhang H, Dai W, He B, Zhang Q and Wang X. The function and mechanism of preactivated thiomers in triggering epithelial tight junctions opening. Eur J Pharm Biopharm 2018; 133: 188-199.
[28] Balda MS, Whitney JA, Flores C, Gonzalez S, Cereijido M and Matter K. Functional dissociation of paracellular permeability and transepithelial electrical resistance and disruption of the apical-basolateral intramembrane diffusion barrier by expression of a mutant tight junction membrane protein. J Cell Biol 1996; 134: 1031-1049.
[29] Reinhold AK and Rittner HL. Barrier function in the peripheral and central nervous system-a review. Pflugers Arch 2017; 469: 123-134.
[30] Czupalla CJ, Liebner S and Devraj K. In vitro models of the blood-brain barrier. Methods Mol Biol 2014; 1135: 415-437.
[31] Poenar DP, Yang G, Wan WK and Feng S. Low-cost method and biochip for measuring the Trans-Epithelial Electrical Resistance (TEER) of esophageal epithelium. Materials (Basel) 2020; 13: 2354.
[32] Sutton SC, Forbes AE, Cargill R, Hochman JH and LeCluyse EL. Simultaneous in vitro measurement of intestinal tissue permeability and transepithelial electrical resistance (TEER) using Sweetana-Grass diffusion cells. Pharm Res 1992; 9: 316-319.
[33] Matter K and Balda MS. Functional analysis of tight junctions. Methods 2003; 30: 228-234.
[34] Rozov A, Khusainov I, El Omari K, Duman R, Mykhaylyk V, Yusupov M, Westhof E, Wagner A and Yusupova G. Importance of potassium ions for ribosome structure and function revealed by long-wavelength X-ray diffraction. Nat Commun 2019; 10: 2519.
[35] Holm RH, Kennepohl P and Solomon EI. Structural and functional aspects of metal sites in biology. Chem Rev 1996; 96: 2239-2314.
[36] Sigel A, Sigel H and Sigel RK. Structural and catalytic roles of metal ions in RNA. Met Ions Life Sci 2011; 9: vii-ix.
[37] The American Journal of Physiology. Science 1897; 6: 590.
[38] Serra MJ, Baird JD, Dale T, Fey BL, Retatagos K and Westhof E. Effects of magnesium ions on the stabilization of RNA oligomers of defined structures. RNA 2002; 8: 307-323.
[39] Huang K, Zhou L, Alanis K, Hou J and Baker LA. Imaging effects of hyperosmolality on individual tricellular junctions. Chem Sci 2020; 11: 1307-1315.
[40] Lodemann U, Einspanier R, Scharfen F, Martens H and Bondzio A. Effects of zinc on epithelial barrier properties and viability in a human and a porcine intestinal cell culture model. Toxicol In Vitro 2013; 27: 834-843.
[41] Bialek S and Miller SS. K+ and Cl- transport mechanisms in bovine pigment epithelium that could modulate subretinal space volume and composition. J Physiol 1994; 475: 401-417.
[42] Joseph DP and Miller SS. Apical and basal membrane ion transport mechanisms in bovine retinal pigment epithelium. J Physiol 1991; 435: 439-463.
[43] Nagahama M, Seike S, Ochi S, Kobayashi K and Takehara M. Clostridium perfringens Epsilon-Toxin Impairs the Barrier Function in MDCK Cell Monolayers in a Ca(2+)-Dependent Manner. Toxins (Basel) 2020; 12: 286.